

Evidence of fully-gapped superconductivity in NbReSi: A combined μ SR and NMR study

T. Shang,^{1,*} D. Tay,² H. Su,^{3,4} H. Q. Yuan,^{3,4,5,6} and T. Shiroka^{2,7}

¹Key Laboratory of Polar Materials and Devices (MOE), School of Physics and Electronic Science, East China Normal University, Shanghai 200241, China

²Laboratorium für Festkörperphysik, ETH Zürich, CH-8093 Zürich, Switzerland

³Center for Correlated Matter and Department of Physics, Zhejiang University, Hangzhou 310058, China

⁴Zhejiang Province Key Laboratory of Quantum Technology and Device,

Department of Physics, Zhejiang University, Hangzhou 310058, China

⁵Collaborative Innovation Center of Advanced Microstructures, Nanjing University, Nanjing, 210093, China

⁶State Key Laboratory of Silicon Materials, Zhejiang University, Hangzhou 310058, China

⁷Laboratory for Muon-Spin Spectroscopy, Paul Scherrer Institut, Villigen PSI, Switzerland

We report a comprehensive study of the noncentrosymmetric NbReSi superconductor by means of muon-spin rotation and relaxation (μ SR) and nuclear magnetic resonance (NMR) techniques. NbReSi is a bulk superconductor with $T_c = 6.5$ K, characterized by a large upper critical field, which exceeds the Pauli limit. Both the superfluid density $\rho_{sc}(T)$ (determined via transverse-field μ SR) and the spin-lattice relaxation rate $T_1^{-1}(T)$ (determined via NMR) suggest a nodeless superconductivity (SC) in NbReSi. We also find signatures of multigap SC, here evidenced by the field-dependent muon-spin relaxation rate and the electronic specific-heat coefficient. The absence of spontaneous magnetic fields below T_c , as evinced from zero-field μ SR measurements, indicates a preserved time-reversal symmetry in the superconducting state of NbReSi. Finally, we discuss possible reasons for the unusually large upper critical field of NbReSi, most likely arising from its anisotropic crystal structure.

I. INTRODUCTION

Superconductors whose crystal structures lack an inversion center, known as noncentrosymmetric superconductors (NCSCs), represent an attractive platform for investigating unconventional- and topological superconductivity (SC) [1–11]. Besides SC, noncentrosymmetric materials are among the best candidates for studying also topological phenomena. For example, Weyl fermions were discovered as quasiparticles in Ta(As,P) and Nb(As,P) noncentrosymmetric single crystals [12–16]. In NCSCs, a lack of inversion center sets the scene for a variety of exotic properties, e.g., nodes in the superconducting gap [17–20], multigap SC [21], upper critical fields beyond the Pauli limit [22–24], and breaking of time-reversal symmetry (TRS) in the superconducting state [20, 25–30].

In some NCSCs, the above exotic properties are closely related to admixtures of spin-singlet and spin-triplet superconducting pairing, here tuned by the antisymmetric spin-orbit coupling (ASOC) [1–3]. In most other cases, however, such connection seems very weak and the superconducting properties resemble those of conventional superconductors, characterized by a fully developed energy gap and a preserved TRS. A notable exception is CaPtAs which, below T_c , exhibits both TRS breaking and superconducting gap nodes [20, 31]. In general, the causes behind TRS breaking in NCSCs are not yet fully understood and remain an intriguing open question.

After the discovery of TRS breaking in elementary rhenium and in α -Mn-type Re T superconductors (T = transition metal) [28–30], many other Re-based superconductors have been systematically investigated by means of muon-spin relaxation and rotation (μ SR). Later on, μ SR studies on Re $_{1-x}$ Mo $_x$ alloys ($0 \leq x \leq 1$) revealed that TRS is broken only in cases of a high rhenium content ($x < 0.12$), surprisingly corresponding to simple centrosymmetric structures [32]. For $x > 0.12$, instead, all the Re-Mo alloys

preserve TRS in their superconducting state, independent of the centro- or noncentrosymmetric crystal structure [32]. Recently, the centrosymmetric Re $_3$ B and noncentrosymmetric Re $_7$ B $_3$ superconductors were systematically studied and shown to exhibit nodeless SC with multiple energy gaps [33]. In both cases, the lack of spontaneous magnetic fields below T_c indicates that, unlike in Re T or in elementary rhenium, the TRS is preserved. Such a selective occurrence of TRS breaking in Re-based superconductors, independent of the noncentrosymmetric structure (and thus of ASOC), is puzzling and not yet fully understood, clearly demanding further investigations.

The NbReSi superconductor represents yet another candidate material for studying the TRS breaking effect in the Re-based family of superconductors. NbReSi crystallizes in a hexagonal ZrNiAl-type crystal structure with space group $P\bar{6}2m$ (No. 189) [see inset in Fig. 1(b)] [34]. Although its SC was reported in 1980s [35], its physical properties were systematically studied only recently [24]. As shown in Fig. 1(a), both magnetic-susceptibility and electrical-resistivity data indicate a $T_c = 6.5$ K in NbReSi. The temperature evolution of the upper critical field $H_{c2}(T)$, as established by electrical-resistivity- and heat-capacity measurements, is reported in Fig. 1(b), with $H_{c2}(0)$ being larger than the weak-coupling Pauli limit value (i.e., $1.86k_B T_c = 12.1$ T). This indicates that the effects of paramagnetic limiting may be either reduced or entirely absent in NbReSi and, hence, that it can possibly exhibit unconventional superconductivity.

Although selected properties of NbReSi have been investigated by different techniques [24], at a microscopic level its superconducting properties, in particular, the superconducting order parameter, have not been explored. In this paper, we report on an extensive study of NbReSi carried out mostly by μ SR and nuclear magnetic resonance (NMR) methods, both in its superconducting- and normal states. Despite a noncentrosymmetric crystal structure, NbReSi is shown to be a moderately correlated electron material, which adopts a fully gapped superconducting state with preserved TRS.

* Corresponding authors:
tshang@phy.ecnu.edu.cn

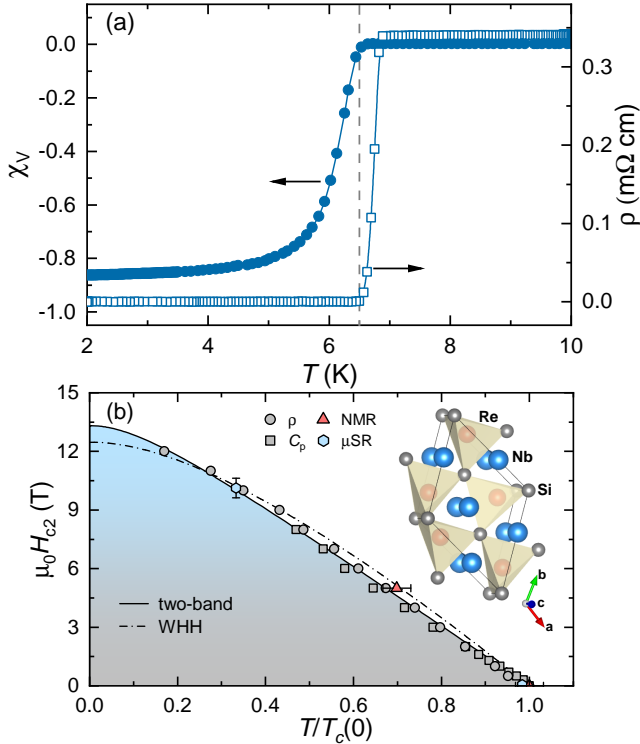


FIG. 1. (a) Temperature-dependent magnetic susceptibility $\chi_V(T)$ (left-axis) and electrical resistivity $\rho(T)$ (right-axis). While $\rho(T)$ was measured in a zero-field condition, $\chi_V(T)$ data were collected in a magnetic field of 1 mT, applied after zero-field cooling (ZFC). The dashed line indicates the $T_c = 6.5$ K. (b) Upper critical field H_{c2} vs reduced temperature $T_c/T_c(0)$ for NbReSi. The solid- and dash-dotted lines represent fits to the two-band- and WHH model. The T_c values determined from μ SR- and NMR measurements (this work) are highly consistent with the values determined from electrical-resistivity- and heat-capacity measurements (data taken from Ref. 24). The inset shows the crystal structure of NbReSi, with the lines marking its unit cell.

II. EXPERIMENTAL DETAILS

Polycrystalline NbReSi samples were prepared by the arc-melting method. The crystal structure and phase purity were checked by powder x-ray diffraction. The bulk SC was characterized by electrical-resistivity-, heat-capacity-, and magnetization measurements [24]. The bulk μ SR measurements were carried out at the multipurpose surface-muon spectrometer (Dolly) of the Swiss muon source at Paul Scherrer Institut, Villigen, Switzerland. In this study, we performed three kinds of experiments: transverse-field (TF)-, zero-field (ZF)-, and longitudinal-field (LF) μ SR measurements. As to the former, it allowed us to determine the temperature evolution of the superfluid density. As to the latter two, we aimed at searching for a possible breaking of time-reversal symmetry in the superconducting state of NbReSi. To exclude the possibility of stray magnetic fields during the ZF- μ SR measurements, all the magnets were preliminarily degaussed. All the μ SR spectra were collected upon heating and were analyzed by means of the `musrfit` software package [36].

^{93}Nb NMR measurements, including line shapes and spin-lattice relaxation times, were performed on NbReSi in powder form in a magnetic field of 5 T. To cover the 2 to 300 K temperature range we used a continuous-flow CF-1200 cryostat by Oxford Instruments, with temperatures below 4.2 K

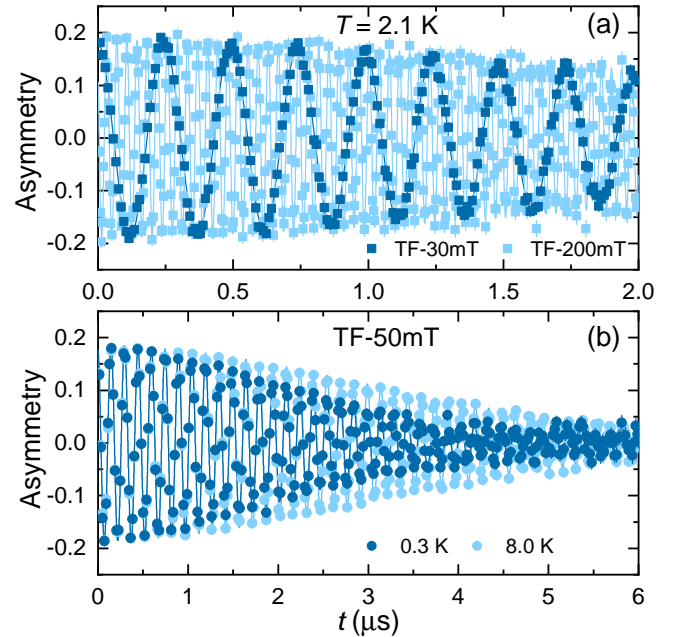


FIG. 2. (a) TF- μ SR spectra of NbReSi collected at $T = 2.1$ K (superconducting state) in a field of 30 and 200 mT. (b) TF- μ SR spectra of NbReSi collected in the superconducting- (0.3 K) and the normal state (8 K) in an applied magnetic field of 50 mT. The solid lines represent fits to Eq. (1). To clearly show the oscillations at higher fields, the spectra in panel (a) are shown in a time range up to 2 μ s.

being achieved under pumped ^4He conditions. Preliminary resonance detuning experiments confirmed the T_c of 6.3 K at 0 T and of 4.4 K at 5 T. The ^{93}Nb NMR signal was detected by means of a standard spin-echo sequence consisting of $\pi/2$ and π pulses of 3 and 6 μ s, with recycling delays ranging from 1 to 60 s in the 2–300 K temperature range. The line-shapes were obtained via fast Fourier transform (FFT) of the echo signal. Spin-lattice relaxation times T_1 were measured via the inversion-recovery method, using a π - $\pi/2$ - π pulse sequence. In all the measurements, phase cycling was used to systematically minimize the presence of artifacts.

III. RESULTS AND DISCUSSION

A. μ SR study

To investigate the superconducting properties of NbReSi at a microscopic level, we carried out systematic temperature-dependent μ SR measurements in a transverse field. The optimal field value for such experiments was determined via preliminary field-dependent μ SR depolarization-rate measurements at 2.1 K. To track the additional field-distribution broadening due to the flux-line lattice (FLL) in the mixed superconducting state, a magnetic field (up to 380 mT) was applied in the normal state and then the sample was cooled down well below T_c , where the μ SR spectra were collected. Figure 2(a) shows two representative TF- μ SR spectra collected at 30 and 200 mT, in general, modeled by:

$$A_{\text{TF}}(t) = A_s e^{-\sigma^2 t^2/2} \cos(\gamma_\mu B_s t + \phi) + A_{\text{bg}} \cos(\gamma_\mu B_{\text{bg}} t + \phi). \quad (1)$$

Here A_s (90%) and A_{bg} (10%) are the sample and the background asymmetries, with the latter not undergoing

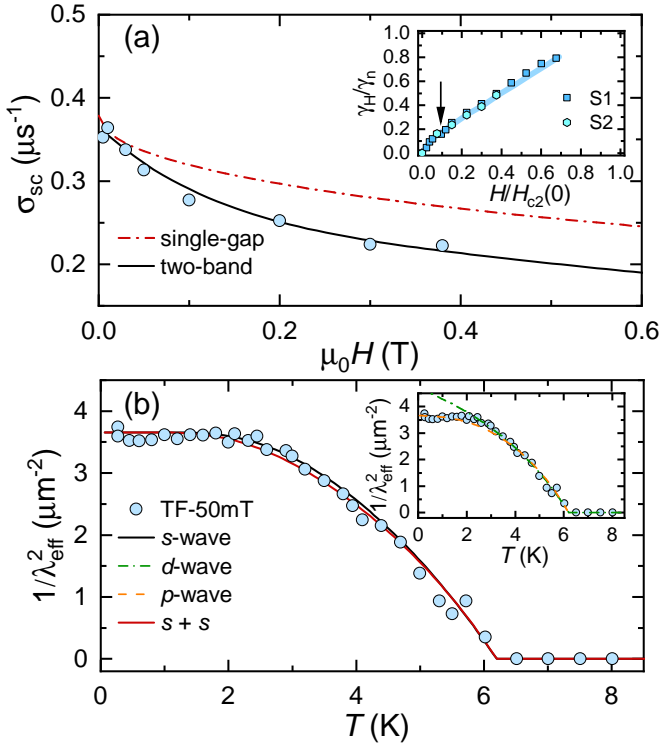


FIG. 3. (a) Field-dependent superconducting Gaussian relaxation rate $\sigma_{sc}(H)$. The dash-dotted and solid lines represent fits to a single-gap and a two-band model. The inset plots the normalized specific-heat coefficient γ_H/γ_n vs the reduced magnetic field $H/H_{c2}(0)$ for NbReSi. At a given applied field, γ_H is obtained as the linear extrapolation of electronic specific heat C_e/T vs T^2 in the superconducting state to zero temperature. Data from different samples (denoted as S1 and S2) are highly consistent. The specific heat data can be found in Ref. 24. The arrow marks a change of slope at $\mu_0 H \sim 1$ T. (b) Temperature dependence of the NbReSi superfluid density. The solid black- and red lines represent fits to a fully-gapped *s*-wave model with one- and two gaps, respectively. The dash-dotted and dashed lines (in the inset) are fits to *p*- and *d*-wave models.

any depolarization. $\gamma_\mu/2\pi = 135.53$ MHz/T is the muon gyromagnetic ratio, B_s and B_{bg} are the local fields sensed by implanted muons in the sample and the sample holder, ϕ is a shared initial phase, and σ is a Gaussian relaxation rate reflecting the field distribution inside the sample. In the superconducting state, the measured σ includes contributions from both the FLL (σ_{sc}) and a smaller, temperature-independent relaxation, due to nuclear moments (σ_n) (see also ZF- μ SR below). The FLL-related relaxation can be extracted by subtracting the nuclear contribution in quadrature, $\sigma_{sc} = \sqrt{\sigma^2 - \sigma_n^2}$.

The resulting superconducting Gaussian relaxation rates σ_{sc} vs the applied external magnetic field are summarized in Fig. 3(a). Above the lower critical field $\mu_0 H_{c1}$ (10.1 mT) [24], the relaxation rate decreases continuously. Here, a field of 50 mT was chosen for the temperature-dependent TF- μ SR studies. In case of a single-gap superconductor, $\sigma_{sc}(H)$ generally follows $\sigma_{sc} = 0.172 \frac{\gamma_\mu \Phi_0}{2\pi} (1-h)[1 + 1.21(1-\sqrt{h})^3]\lambda^{-2}$ [37, 38], where $h = H_{app}/H_{c2}$, with H_{app} being the applied magnetic field. As shown by the dash-dotted line in Fig. 3(a), the single-gap model shows a very poor agreement with the experimental data. In a two-band model, each band is characterized by its own coherence length and a weight w [or $(1-w)$], accounting for

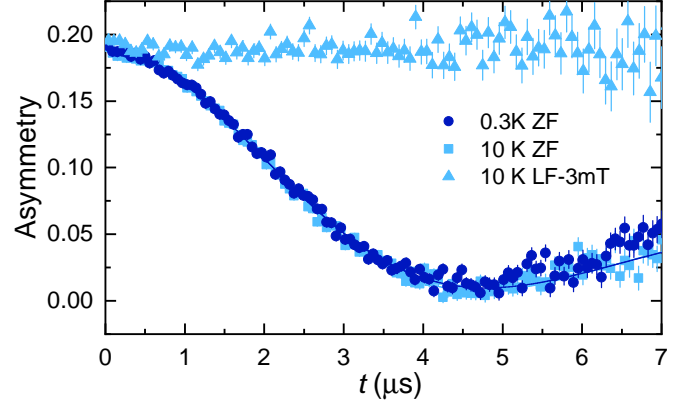


FIG. 4. ZF- μ SR spectra collected in the superconducting- (0.3 K) and the normal (10 K) states for NbReSi. The LF- μ SR in a field of 3 mT was collected at 0.3 K after field cooling.

the relative contribution of each band to the total σ_{sc} and, hence, to the superfluid density [39, 40]. For such a two-band model, the second moment of the field distribution can be calculated within the framework of the modified London model by using the following expression:

$$\langle B^2 \rangle = \frac{\sigma_{sc}^2}{\gamma_\mu^2} = B^2 \sum_{q \neq 0} \left[w \frac{e^{-\frac{q^2 \xi_1^2}{2(1-h_1)}}}{1 + \frac{q^2 \lambda_0^2}{1-h_1}} + (1-w) \frac{e^{-\frac{q^2 \xi_2^2}{2(1-h_2)}}}{1 + \frac{q^2 \lambda_0^2}{1-h_2}} \right]^2. \quad (2)$$

Here, $q = 4\pi/\sqrt{3}a(m\sqrt{3}/2, n+m/2)$ are the reciprocal lattice vectors for a hexagonal FLL (a is the inter-vortex distance, m and n are integer numbers); $B = \mu_0 H$ for $H \gg H_{c1}$, which is the mean field within the FLL; $h_{1(2)} = H/H_{c2,1(2)}$ are the reduced fields within band 1(2) (the same as h in the above equation) and $\xi_{1(2)}$ are the coherence lengths for the band 1(2). As shown by the solid line in Fig. 3(a), with $w = 0.45$, the two-band model is in good agreement with the experimental data and provides $\lambda_0 = 534(2)$ nm, $\xi_1 = 18.0(5)$ nm, and $\xi_2 = 5.7(2)$ nm. The derived λ_0 is comparable with the value estimated from the temperature-dependent TF- μ SR measurements in Fig. 3(b). The upper critical field of 10.1(5) T, calculated from the coherence length of the second band, $\mu_0 H_{c2} = \Phi_0/(2\pi\xi_2^2)$, is highly consistent with the upper critical field determined from bulk measurements [see Fig. 1(b)] (The specific-heat data were taken from Ref. 24). The *virtual* upper critical field $\mu_0 H_{c2}^* = 1.02(6)$ T, calculated from the coherence length of the first band ξ_1 , is in good agreement with the field value where $\gamma_H(H)$ shows a change in slope [as indicated by an arrow in the inset of Fig. 3(a)]. The *virtual* H_{c2}^* corresponds to the critical field which suppresses the small superconducting gap. Clearly, both the field-dependent $\sigma_{sc}(H)$ and the electronic specific-heat coefficient $\gamma_H(H)$ suggest the existence of multiple superconducting gaps in NbReSi.

To further investigate the superconducting pairing in NbReSi, we carried out systematic TF- μ SR measurements in an applied field of 50 mT over a wide temperature range. Representative TF- μ SR spectra collected in the superconducting (0.3 K)- and normal (8 K) state of NbReSi are shown in Fig. 2(b). The broadening of the field distribution due to FLL is clearly visible in the superconducting state. To quantify it, the TF- μ SR spectra were analyzed using again the model given by Eq. (1). In NbReSi, the upper critical field H_{c2} is very large compared to the applied TF field

(50 mT). Therefore, the effects of overlapping vortex cores with increasing field can be ignored when extracting the penetration depth from the measured σ_{sc} . The effective magnetic penetration depth λ_{eff} can be calculated from $\sigma_{sc}^2(T)/\gamma_\mu^2 = 0.00371 \Phi_0^2/\lambda_{eff}^4(T)$ [37, 38]. Figure 3(b) summarizes the temperature-dependent inverse square of the magnetic penetration depth, which is proportional to the superfluid density, i.e., $\lambda_{eff}^{-2}(T) \propto \rho_{sc}(T)$. The latter was then analyzed by means of different models, generally described by:

$$\rho_{sc}(T) = 1 + 2 \left\langle \int_{\Delta_k}^{\infty} \frac{E}{\sqrt{E^2 - \Delta_k^2}} \frac{\partial f}{\partial E} dE \right\rangle_{FS}. \quad (3)$$

Here, $f = (1 + e^{E/k_B T})^{-1}$ is the Fermi function and $\langle \rangle_{FS}$ represents an average over the Fermi surface [41]. $\Delta_k(T) = \Delta(T)\delta_k$ is an angle-dependent gap function, where Δ is the maximum gap value and δ_k is the angular dependence of the gap, equal to 1, $\cos 2\phi$, and $\sin \theta$ for an s -, d -, and p -wave model, respectively, with ϕ and θ being the azimuthal angles. The temperature dependence of the gap is assumed to follow $\Delta(T) = \Delta_0 \tanh\{1.82[1.018(T_c/T - 1)]^{0.51}\}$ [41, 42], where Δ_0 is the gap value at 0 K.

Four different models, including single-gap s -, p -, and d -wave, and two-gap $s + s$ -wave, were used to describe the $\lambda_{eff}^{-2}(T)$ data. For an s - or p -wave model, the best fits yield the same zero-temperature magnetic penetration depth $\lambda_0 = 523(2)$ nm, but different gap values, 1.04(3) and 1.33(5) meV, respectively. Note that, $\rho_{sc}(T)$ is also consistent with a dirty-limit model [33], which yields a similar superconducting gap [i.e., 0.93(3) meV]. For the d -wave model, the estimated λ_0 and gap value are 460(4) nm and 1.28(5) meV.

As can be clearly seen in the inset of Fig. 3(b), the significant deviation of the p - or d -wave model from the experimental data below ~ 3 K and the temperature-independent behavior of $\lambda_{eff}^{-2}(T)$ for $T < 1/3 T_c \sim 2$ K strongly suggest a fully-gapped superconductivity in NbReSi. Since $H_{c2}(T)$, $\sigma_{sc}(H)$, and $\gamma_H(H)$ data [see Fig. 1(b) and Fig. 3(a)] imply the presence of multiple superconducting gaps in NbReSi, $\lambda_{eff}^{-2}(T)$ was also analyzed using a two-gap s -wave model. In this case, $\rho_{sc}(T) = w\rho_{sc}^{\Delta_{0,1}}(T) + (1-w)\rho_{sc}^{\Delta_{0,2}}(T)$, with $\rho_{sc}^{\Delta_{0,1}}$ and $\rho_{sc}^{\Delta_{0,2}}(T)$ being the superfluid densities related to the first- ($\Delta_{0,1}$) and second ($\Delta_{0,2}$) gap, and w a relative weight. Here, by fixing the weight $w = 0.45$, as determined from $\sigma_{sc}(H)$, the two-gap $s + s$ -wave model provides almost identical results to the single-gap s -wave model, reflected in two practically overlapping fitting curves in Fig. 3(b). The two-gap model yields $\Delta_{0,1} = 0.80(5)$ meV and $\Delta_{0,2} = 1.23(5)$ meV. Since the gap sizes are not significantly different ($\Delta_{0,1}/\Delta_{0,2} \sim 0.7$), this makes it difficult to discriminate between a single- and a two-gap superconductor based on the temperature-dependent superfluid density alone [40, 43]. Nevertheless, as we show above, the two-gap feature in NbReSi is clearly reflected in its field-dependent superconducting relaxation rate $\sigma_{sc}(H)$, specific-heat coefficient $\gamma_H(H)$, and also in the temperature-dependent upper critical field $H_{c2}(T)$. The superconducting gap of NbReSi derived from TF- μ SR is similar to that of other Re-based superconductors, e.g., ReT (T = transition metal) [29, 30, 32, 44, 45] and rhenium-boron compounds [46], the latter exhibiting a multigap SC, too.

To search for a possible breaking of the time-reversal symmetry in the superconducting state of NbReSi, we compared

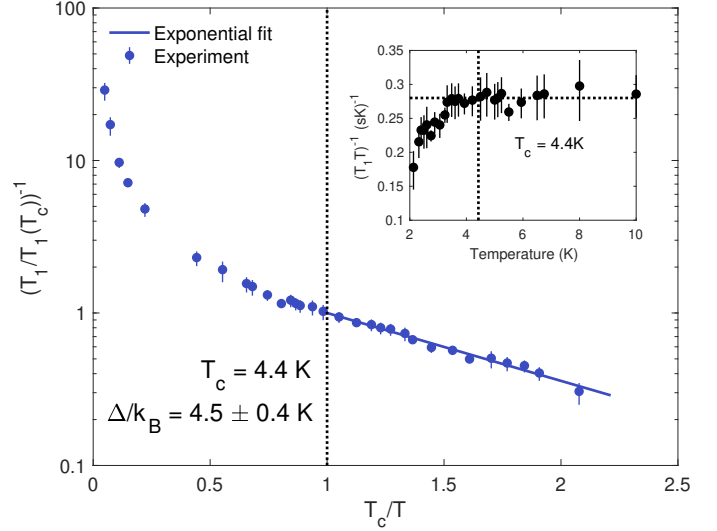


FIG. 5. The NMR relaxation rate T_1^{-1} as a function of temperature (here measured at $\mu_0 H = 5$ T) decays by following an exponential law, $T_1^{-1} \propto \exp(-\Delta/k_B T)$, typical of s -wave superconductivity with a fixed gap Δ . The vertical line at 1 refers to the T_c value at 5 T. Inset: Korringa product $(T_1 T)^{-1}$ as a function of temperature. Its constant value above T_c [here, ca. 0.28 (sK) $^{-1}$] indicates an ideal metallic behavior, followed by a gradual decrease below the superconducting transition. The T_c value determined from $(T_1 T)^{-1}$ is consistent those obtained by other techniques [see Fig. 1(b)]

the ZF- μ SR results in the normal- and superconducting states. As shown in Fig. 4, neither coherent oscillations nor fast decays could be identified in the spectra collected above (10 K) and below T_c (0.3 K), hence implying the lack of any magnetic order or fluctuations. Normally, in the absence of external fields, the onset of SC does not imply any changes in the ZF muon-spin relaxation rate. However, if the TRS is broken, the onset of spontaneous magnetic fields can be detected by ZF- μ SR as an increase in the muon-spin relaxation rate. In absence of external fields, the muon-spin relaxation is mainly attributed to the randomly oriented nuclear moments, which can be modeled by means of a phenomenological relaxation function, consisting of a combination of Gaussian- and Lorentzian Kubo-Toyabe relaxations [47, 48],

$$A(t) = A_s \left[\frac{1}{3} + \frac{2}{3} (1 - \sigma_{ZF}^2 t^2 - \Lambda_{ZF} t) e^{(-\frac{\sigma_{ZF}^2 t^2}{2} - \Lambda_{ZF} t)} \right] + A_{bg}.$$

Here, A_s and A_{bg} are the same as in the TF- μ SR case [see Eq. (1)]. The σ_{ZF} and Λ_{ZF} represent the zero-field Gaussian and Lorentzian relaxation rates, respectively. As shown by the solid lines in Fig. 4, the derived relaxations in the normal- and the superconducting states are almost identical. This lack of evidence for an additional μ SR relaxation below T_c excludes a possible TRS breaking in the superconducting state of NbReSi.

B. ^{93}Nb NMR study

NMR is a versatile technique for investigating the electronic properties of materials, in particular, their electron correlations, complementary to μ SR with respect to the probe location, coupling to the environment, time window, and field range. Here we employed NMR to investigate the normal- and superconducting-state properties of NbReSi, mostly via ^{93}Nb NMR measurements in a field of 5 T. In

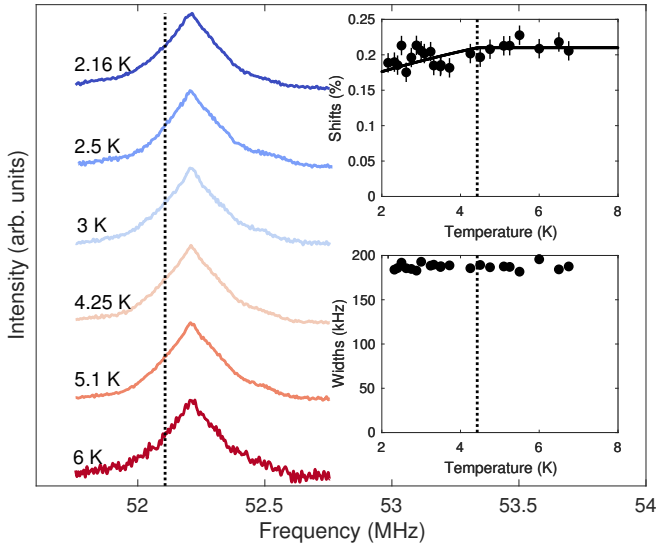


FIG. 6. ^{93}Nb NMR lineshapes collected at various temperatures, covering both the superconducting- and normal states, in a magnetic field of 5 T. The dashed line indicates the reference frequency. The derived NMR Knight shifts and widths vs temperature are shown in the insets. While Knight shifts show a negligible drop below T_c , the line widths are independent of temperature.

selected cases, we conducted also ^{29}Si NMR ($I = 1/2$) measurements. In either case, the NMR reference frequency ν_0 was determined from the ^{27}Al resonance signal in an $\text{Al}(\text{NO}_3)_3$ solution [49]. Successively, the ^{93}Nb (or ^{29}Si) NMR shifts were calculated with respect to each ν_0 reference frequency. Considering its good NMR signal and fast relaxation rate, ^{93}Nb was used as the nucleus of choice for investigating the electronic properties of NbReSi. The NMR line shapes shown in Fig. 6 most likely represent the central transition line and are characterized by a relatively large width (ca. 200 kHz). No satellite transitions were observed within 1 MHz on either side of the central transition line, indicating that quadrupolar coupling is either extremely weak (satellites located within the linewidth of the central line) or extremely large (satellites located at ≥ 1 MHz away from the central transition). Considering the complex and asymmetric coordination of Nb atoms, we expect the latter to be the case [50][51]. The central NMR line is sufficient for investigating the superconducting properties of NbReSi.

Two main conclusions can be drawn from our NMR study. Firstly, the temperature dependence of the Korringa product indicates a transition from the metallic to the superconducting phase. Secondly, the exponential dependence of relaxation rate in the superconducting phase confirms the occurrence of a fully-gapped SC phase. Our detailed findings are elaborated on below.

To determine the $T_c(H)$ of NbReSi, we use a standard detuning method (see Fig. 7), which gives $T_c(5\text{ T}) = 4.4\text{ K}$. The superconducting transition is also confirmed by the Korringa product in the ^{93}Nb case (see inset in Fig. 5) [52]. Above T_c , we observe an ideal behavior [i.e., $(T_1 T)^{-1}$ constant], typical of standard metals. As the temperature drops below $T_c = 4.4\text{ K}$, we observe a gradual decrease of the $(T_1 T)^{-1}$ product, reflecting a slowing down of the relaxation rate due to electron pairing, a key signature of the superconducting state.

To determine the nature of the superconducting gap, we turn to the relaxation-rate data. The relaxation of

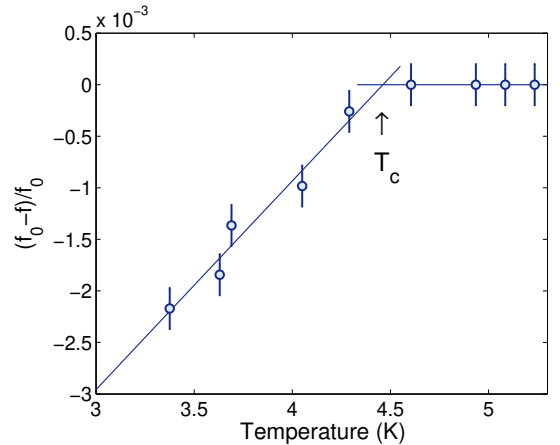


FIG. 7. Frequency detuning of the NMR resonant circuit with temperature. At the onset of superconductivity at $T_c(5\text{ T}) = 4.4\text{ K}$ the magnetic flux is (partially) expelled, equivalent to a lowering of inductance, and hence to an increase in frequency $f = 1/(2\pi\sqrt{LC})$.

^{93}Nb nuclei can be modeled by an exponential function $T_1^{-1} \propto \exp(-\Delta/k_B T)$ (see Fig. 5). The fit provides a temperature-independent gap $\Delta/k_B = 4.5 \pm 0.9\text{ K}$ (equivalent to $\Delta/k_B T_c = 1.02$), lower than that determined by other techniques, most likely reflecting an important quadrupole contribution to relaxation. Independent of the gap value, the exponential decrease of relaxation can be interpreted as a critical slowing down of the electronic spin fluctuations. The fact that the superconducting gap is constant and temperature independent provides strong evidence of conventional s -wave superconductivity in NbReSi, although NMR is not sensitive enough to distinguish single- from multigap SC. Since unconventional superconductivity would give rise to a power-law-dependent relaxation rate vs. temperature (see, e.g., Ref. 53), the exponential decrease of relaxation is sufficient to prove that the system possesses a fully-opened gap. Nevertheless, for completeness, below we discuss some surprising aspects that, although unexpected, can still be reconciled with the theory of conventional SC.

It is surprising that the NMR relaxation data do not exhibit a Habel-Slichter (HS) peak just below the superconducting transition, a typical feature of most s -wave superconductors. Several factors might account for the suppression of the HS peak. Firstly, the impurities may play a role in the reduction of the HS peak, which might also lead to the weak temperature dependence of NMR shifts [54]. Secondly, the HS peak can be smeared out by quadrupole effects, considering that ^{93}Nb has $I = 9/2$. This smearing has been observed in other noncentrosymmetric superconductors with an s -wave gap (for instance, $\text{W}_3\text{Al}_2\text{C}$ shows an HS peak in the $I = 1/2$ ^{13}C relaxation, but none in that of $I = 5/2$ ^{27}Al [55]). To disentangle the contribution of quadrupole effects to the relaxation rate, one has to either measure the same system at lower fields or resort to non-quadrupolar nuclei (here, ^{29}Si). The almost quadratic decrease of the signal-to-noise ratio with field [56] and the appearance of acoustic ringing at low frequencies make this route unpractical. On the other hand, numerical calculations suggest that the density of states at Fermi level is dominated by the Re-5d and Nb-4d orbitals, the contribution of Si orbitals being negligible [24]. Hence, we expect a much weaker magnetic hyperfine coupling to ^{29}Si - than to ^{93}Nb nuclei, corresponding to a much slower relaxation in the former case. Indeed, experimentally we

find that, in NbReSi, the relaxation rate of ^{29}Si nuclei is prohibitively slow (~ 30 s at 4 K, becoming exponentially slower below T_c), thus making the use of ^{29}Si nuclei unfeasible for probing the nuclear relaxation in the superconducting state.

It is also surprising that both the line shift and width (see Fig. 6) are almost constant with temperature, with the line shapes above and below T_c being virtually indistinguishable. The insensitivity of the line shift to the superconducting transition, at first seems to suggest a spin-triplet pairing, where electron spins maintain their mutual orientation across T_c . However, this apparent contradiction is resolved by a comparison with well-known transition-metal superconductors. Indeed, as has been shown for tin, vanadium, niobium, etc., their total shift is given as the sum of spin- and orbital components $K = K_s + K_{\text{orb}}$, with K_{orb} being the dominant contribution [57]. As the latter is unaffected by the electron-spin pairing in the superconducting state, this accounts for an almost constant NMR shift across T_c , yet compatible with a standard s -wave pairing. Indeed, as shown in Fig. 6, we observe a negligible decrease in frequency, which could indicate that $K_s \ll K_{\text{orb}}$. Other mechanisms, such as disorder, could account for the almost constant NMR shift across T_c . Indeed, in strongly-coupled systems, even tiny amounts of impurities can lead to temperature-independent shifts [54]. Last but not least, sample-heating effects caused by eddy currents might also play a role in reducing the observed line shift [58]. However, such effects are normally relevant only at very low temperatures in good conducting samples (i.e., able to sustain eddy currents), or for fast pulse-repetition rates. Since neither the sample nor the measurement conditions fully satisfy such requirements, it is unlikely that sample heating might explain the weak Knight shifts in NbReSi. In general, although some questions about the role of quadrupole interactions and disorder in suppressing the HS peak remain open, the exponential dependence of the relaxation rate below T_c unambiguously proves the existence of fully-gapped superconductivity in NbReSi.

C. Discussion

According to TF- μ SR measurements at various temperatures, the superfluid density $\rho_{\text{sc}}(T)$ shows an almost temperature-independent behavior below $1/3 T_c$ [see Fig. 3(b)], indicating the absence of low-energy excitations and thus, a nodeless SC in NbReSi. Both the single-gap s - and two-gap $s + s$ -wave models describe the $\rho_{\text{sc}}(T)$ data very well. However, the field-dependent superconducting Gaussian relaxation rate $\sigma_{\text{sc}}(H)$ and the electronic specific-heat coefficient $\gamma_{\text{H}}(H)$ [see Fig. 3(a)] provide clear evidence of multigap SC in NbReSi, both datasets showing a distinct field response compared to a single-gap superconductor [33, 59, 60]. As indicated by the arrow in the inset of Fig. 3(a), $\gamma_{\text{H}}(H)$ exhibits a clear change in slope when the applied magnetic field (larger than 1 T) suppresses the small gap, a feature recognized as the fingerprint of multigap superconductors. Conversely, $\gamma_{\text{H}}(H)$ would be mostly linear in the single-gap case. Moreover, a single-gap model cannot describe the $\sigma_{\text{sc}}(H)$ data [see main panel of Fig. 3(a)]. At the same time, the two-band model yields an upper critical field $\mu_0 H_{c2}(2.1 \text{ K}) = 10.1 \text{ T}$, consistent with the value determined from other techniques. The derived *virtual* upper critical field $\mu_0 H_{c2}^* = 1.02 \text{ T}$ is in good agreement with the field value where $\gamma_{\text{H}}(H)$ shows a change in slope. Here,

H_{c2}^* corresponds to the critical field which suppresses the small superconducting gap. The multigap SC of NbReSi can be further inferred from the temperature-dependent upper critical field $H_{c2}(T)$. As shown in Fig. 1(b), the two-band model [61] is clearly superior to the Werthamer-Helfand-Hohenberg (WHH) model [62] over the whole temperature range. The analysis of $H_{c2}(T)$ with the two-band model indicates that the intra-band and inter-band couplings are $\lambda_{11} \sim \lambda_{22} = 0.17$ and $\lambda_{12} = 0.1$, respectively. As the inter-band coupling is not much different from intra-band coupling, this makes the SC gaps belonging to different electronic bands less distinguishable [63]. In addition, as has been found in other multigap superconductors [33, 40, 59, 60], a relatively small weight of the second gap, or gap sizes not significantly different, make it difficult to discriminate between a single- and a two-gap superconductor from the temperature-dependent superconducting properties only. However, in the NbReSi case, also the electronic band-structure calculations support a multigap SC, since they indicate that more than four bands cross the Fermi level [24].

The two-band model leads to an upper critical field $\mu_0 H_{c2}(0) = 13.3 \text{ T}$, which is beyond the weak-coupling Pauli value, i.e., $1.86 k_{\text{B}} T_c = 12.1 \text{ T}$. In NCSCs, the antisymmetric spin-orbit coupling allows for the occurrence of an admixture of singlet and triplet pairings, which in turn can enhance the upper critical field. Consequently, in this case, a violation of the Pauli limit hints at the presence of unconventional SC. Although in NbReSi the band splitting near the Fermi level is relatively large compared to other NCSCs (i.e., $E_{\text{ASOC}} \sim 180 \text{ meV}$) [1, 2, 24], its superconducting pairing is more consistent with spin-singlet, here reflected in a fully-gapped superconducting state. Indeed, the temperature-dependent zero-field electronic specific heat $C_e(T)/T$, superfluid density $\rho_{\text{sc}}(T)$, and NMR spin relaxation rate $T_1^{-1}(T)$ all suggest a nodeless SC in NbReSi. Furthermore, the preserved TRS below T_c , as revealed by ZF- μ SR, suggests the absence of spin-triplet pairing in NbReSi. Therefore, the enhanced H_{c2} of NbReSi is unlikely to be caused by a mixed-type of pairing. Strong electron correlations can also lead to a large H_{c2} , e.g., the noncentrosymmetric CePt₃Si and Ce(Rh,Ir)Si₃ exhibit H_{c2} values far beyond the Pauli limit [23, 64, 65]. In NbReSi, however, both the temperature-independent Korrington product $(T_1 T)^{-1}$ in the normal state and the small electronic specific-heat coefficient ($\gamma_{\text{n}} \sim 8.23 \text{ mJ/mol-K}^2$ [24]) suggest weak electron correlations. A large superconducting gap value or a strong electron-phonon coupling may also enhance H_{c2} [1, 66]. However, the estimated electron-phonon coupling $\lambda_{\text{ep}} = 0.66$ is rather weak in NbReSi [24], while its gap value $\Delta_0 = 1.95 k_{\text{B}} T_c$, as determined from TF- μ SR [see Fig. 3(b)], is not much larger than the BCS weak-coupling value (i.e., $1.76 k_{\text{B}} T_c$).

Having excluded some common causes of a large H_{c2} , we examine now the role of anisotropy, considering that a highly anisotropic structure can often lead to a sizeable H_{c2} . For instance, in the quasi-one-dimensional Cr-based $A_2\text{Cr}_3\text{As}_3$ ($A = \text{K, Rb, and Cs}$) superconductors, despite T_c s in the 2 to 6 K range, upper critical fields up to 40 T have been reported [67–71]. Although triplet pairing was proposed in $A_2\text{Cr}_3\text{As}_3$ [72–74], a violation of the Pauli limit is also possible for singlet SC. In this case, the spins of Cooper pairs are aligned predominantly along the Cr chains, which play the role of the easy magnetization axis, but cause no magnetic order in the normal paramagnetic state. This scenario is consistent with the presence of Pauli-limiting

pair breaking and the strong $H_{c2}(T)$ anisotropy observed in $K_2Cr_3As_3$ [67]. NbReSi adopts a hexagonal crystal structure ($P62m$, No. 189, with in-plane and out-of-plane lattice parameters $a = 6.7194 \text{ \AA}$ and $c = 3.4850 \text{ \AA}$), which is very similar to the crystal structure of $A_2Cr_3As_3$ ($P\bar{6}m2$, No. 187). Both structures lack an inversion center and have a D_{3h} point group. Therefore, the large H_{c2} of NbReSi is most likely related to its anisotropic crystal structure. Such scenario is indirectly supported by the fact that the sister compound TaReSi, which also adopts a noncentrosymmetric crystal structure (space group $Ima2$, No. 46), but is less anisotropic [75], exhibits a relatively small upper critical field, $\mu_0 H_{c2}(0) = 6.6 \text{ T}$. To clarify the role of anisotropy in enhancing H_{c2} , measurements on NbReSi single crystals are highly desirable. Besides the above intrinsic effects, also extrinsic effects may enhance the H_{c2} of NbReSi. For instance, as previously reported in MgB_2 , single crystals exhibit a $H_{c2}(0)$ up to 18 T [76], while a sizable impurity scattering introduced by disorder significantly enhances this value up to almost 50 T [77]. To exclude (or confirm) this possibility, again, measurements on high-quality single crystals are required. Although to date NbReSi single crystals are not available, future work on crystal growth could make them accessible.

IV. CONCLUSION

To summarize, we studied the superconducting properties of the noncentrosymmetric NbReSi superconductor by means of the μ SR and NMR techniques. The superconducting state of NbReSi is characterized by $T_c = 6.5 \text{ K}$ and

an upper critical field $\mu_0 H_{c2}(0) = 13.3 \text{ T}$. The temperature-dependent superfluid density and the NMR spin-lattice relaxation rate reveal a *nodeless* superconductivity, well described by an *isotropic s-wave* model. The NMR Knight shift exhibits only a negligible drop below T_c , most likely due to a dominant orbital contribution. Field-dependent measurements, including muon-spin relaxation and electronic specific-heat coefficient, imply the presence of multiple superconducting gaps in NbReSi. This is also supported by the temperature dependence of the upper critical field $H_{c2}(T)$. The lack of spontaneous magnetic fields below T_c indicates that, unlike in ReT or elementary rhenium superconductors, time-reversal symmetry is *preserved* in the superconducting state of NbReSi. In general, the μ SR and the NMR relaxation-rate results are highly consistent with a spin-singlet pairing in NbReSi. Finally, the violation of Pauli limit in NbReSi is most likely related to its anisotropic crystal structure rather than to an unconventional type of pairing.

ACKNOWLEDGMENTS

This work was supported from the Natural Science Foundation of Shanghai (Grant Nos. 21ZR1420500 and 21JC1402300) and the Schweizerische Nationalfonds zur Förderung der Wissenschaftlichen Forschung (SNF) (Grant Nos. 200021_188706 and 206021_139082). H.Q.Y. acknowledge support from the National Key R&D Program of China (No. 2017YFA0303100 and No. 2016YFA0300202), the Key R&D Program of Zhejiang Province, China (No. 2021C01002), the National Natural Science Foundation of China (No. 11974306). We acknowledge the allocation of beam time at the Swiss muon source, and thank the scientists of Dolly μ SR spectrometer for their support.

-
- [1] E. Bauer and M. Sigrist, eds., *Non-Centrosymmetric Superconductors*, Vol. 847 (Springer Verlag, Berlin, 2012).
 - [2] M. Smidman, M. B. Salamon, H. Q. Yuan, and D. F. Agterberg, Superconductivity and spin-orbit coupling in noncentrosymmetric materials: A review, *Rep. Prog. Phys.* **80**, 036501 (2017).
 - [3] S. K. Ghosh, M. Smidman, T. Shang, J. F. Annett, A. D. Hillier, J. Quintanilla, and H. Yuan, Recent progress on superconductors with time-reversal symmetry breaking, *J. Phys.: Condens. Matter* **33**, 033001 (2020).
 - [4] H. Kim, K. Wang, Y. Nakajima, R. Hu, S. Ziemak, P. Syers, L. Wang, H. Hodovanets, J. D. Denlinger, P. M. R. Brydon, D. F. Agterberg, M. A. Tanatar, R. Prozorov, and J. Paglione, Beyond triplet: Unconventional superconductivity in a spin-3/2 topological semimetal, *Sci. Adv.* **4**, eaao4513 (2018).
 - [5] Z. X. Sun, M. Enayat, A. Maldonado, C. Lithgow, E. Yelland, D. C. Peets, A. Yaresko, A. P. Schnyder, and P. Wahl, Dirac surface states and nature of superconductivity in noncentrosymmetric BiPd, *Nat. Commun.* **6**, 6633 (2015).
 - [6] M. N. Ali, Q. D. Gibson, T. Klimczuk, and R. J. Cava, Noncentrosymmetric superconductor with a bulk three-dimensional Dirac cone gapped by strong spin-orbit coupling, *Phys. Rev. B* **89**, 020505(R) (2014).
 - [7] M. Sato and S. Fujimoto, Topological phases of noncentrosymmetric superconductors: Edge states, Majorana fermions, and non-Abelian statistics, *Phys. Rev. B* **79**, 094504 (2009).
 - [8] Y. Tanaka, Y. Mizuno, T. Yokoyama, K. Yada, and M. Sato, Anomalous Andreev bound state in noncentrosymmetric superconductors, *Phys. Rev. Lett.* **105**, 097002 (2010).
 - [9] M. Sato and Y. Ando, Topological superconductors: A review, *Rep. Prog. Phys.* **80**, 076501 (2017).
 - [10] X.-L. Qi and S.-C. Zhang, Topological insulators and superconductors, *Rev. Mod. Phys.* **83**, 1057 (2011).
 - [11] C. Kallin and J. Berlinsky, Chiral superconductors, *Rep. Prog. Phys.* **79**, 054502 (2016).
 - [12] S.-Y. Xu, I. Belopolski, N. Alidoust, M. Neupane, G. Bian, C. Zhang, R. Sankar, G. Chang, Z. Yuan, C.-C. Lee, S.-M. Huang, H. Zheng, J. Ma, D. S. Sanchez, B. Wang, A. Bansil, F. Chou, P. P. Shibayev, H. Lin, S. Jia, and M. Z. Hasan, Discovery of a Weyl fermion semimetal and topological Fermi arcs, *Science* **349**, 613 (2015).
 - [13] S.-Y. Xu, N. Alidoust, I. Belopolski, Z. Yuan, G. Bian, T.-R. Chang, H. Zheng, V. N. Strocov, D. S. Sanchez, G. Chang, *et al.*, Discovery of a Weyl fermion state with Fermi arcs in niobium arsenide, *Nat. Phys.* **11**, 748 (2015).
 - [14] B. Q. Lv, H. M. Weng, B. B. Fu, X. P. Wang, H. Miao, J. Ma, P. Richard, X. C. Huang, L. X. Zhao, G. F. Chen, Z. Fang, X. Dai, T. Qian, and H. Ding, Experimental discovery of Weyl semimetal TaAs, *Phys. Rev. X* **5**, 031013 (2015).
 - [15] N. Xu, H. M. Weng, B. Q. Lv, C. E. Matt, J. Park, F. Bisti, V. N. Strocov, D. Gawryluk, E. Pomjakushina, K. Conder, N. C. Plumb, M. Radovic, G. Autés, O. V. Yazyev, Z. Fang, X. Dai, T. Qian, J. Mesot, H. Ding, and M. Shi, Observation of Weyl nodes and Fermi arcs in tantalum phosphide, *Nat. Commun.* **7**, 11006 (2016).
 - [16] S. Souma, Z. Wang, H. Kotaka, T. Sato, K. Nakayama, Y. Tanaka, H. Kimizuka, T. Takahashi, K. Yamauchi, T. Oguchi, K. Segawa, and Y. Ando, Direct observation of nonequivalent

- Fermi-arc states of opposite surfaces in the noncentrosymmetric Weyl semimetal NbP, *Phys. Rev. B* **93**, 161112(R) (2016).
- [17] H. Q. Yuan, D. F. Agterberg, N. Hayashi, P. Badica, D. Vandervelde, K. Togano, M. Sigrist, and M. B. Salamon, *s*-wave spin-triplet order in superconductors without inversion symmetry: $\text{Li}_2\text{Pd}_3\text{B}$ and $\text{Li}_2\text{Pt}_3\text{B}$, *Phys. Rev. Lett.* **97**, 017006 (2006).
- [18] M. Nishiyama, Y. Inada, and G.-q. Zheng, Spin triplet superconducting state due to broken inversion symmetry in $\text{Li}_2\text{Pt}_3\text{B}$, *Phys. Rev. Lett.* **98**, 047002 (2007).
- [19] I. Bonalde, W. Brämer-Escamilla, and E. Bauer, Evidence for line nodes in the superconducting energy gap of noncentrosymmetric CePt_3Si from magnetic penetration depth measurements, *Phys. Rev. Lett.* **94**, 207002 (2005).
- [20] T. Shang, M. Smidman, A. Wang, L.-J. Chang, C. Baines, M. K. Lee, Z. Y. Nie, G. M. Pang, W. Xie, W. B. Jiang, M. Shi, M. Medarde, T. Shiroka, and H. Q. Yuan, Simultaneous nodal superconductivity and time-reversal symmetry breaking in the noncentrosymmetric superconductor CaPtAs , *Phys. Rev. Lett.* **124**, 207001 (2020).
- [21] S. Kuroiwa, Y. Saura, J. Akimitsu, M. Hiraishi, M. Miyazaki, K. H. Satoh, S. Takeshita, and R. Kadono, Multigap superconductivity in sesquicarbides La_2C_3 and Y_2C_3 , *Phys. Rev. Lett.* **100**, 097002 (2008).
- [22] E. M. Carnicom, W. Xie, T. Klimczuk, J. J. Lin, K. Górnicka, Z. Sobczak, N. P. Ong, and R. J. Cava, TaRh_2B_2 and NbRh_2B_2 : Superconductors with a chiral noncentrosymmetric crystal structure, *Sci. Adv.* **4**, eaar7969 (2018).
- [23] E. Bauer, G. Hilscher, H. Michor, C. Paul, E. W. Scheidt, A. Gribanov, Y. Seropegin, H. Noël, M. Sigrist, and P. Rogl, Heavy fermion superconductivity and magnetic order in noncentrosymmetric CePt_3Si , *Phys. Rev. Lett.* **92**, 027003 (2004).
- [24] H. Su, T. Shang, F. Du, C. F. Chen, H. Q. Ye, X. Lu, C. Cao, M. Smidman, and H. Q. Yuan, NbReSi : A noncentrosymmetric superconductor with large upper critical field, *Phys. Rev. Mater.* **5**, 114802 (2021).
- [25] A. D. Hillier, J. Quintanilla, and R. Cywinski, Evidence for time-reversal symmetry breaking in the noncentrosymmetric superconductor LaNiC_2 , *Phys. Rev. Lett.* **102**, 117007 (2009).
- [26] J. A. T. Barker, D. Singh, A. Thamizhavel, A. D. Hillier, M. R. Lees, G. Balakrishnan, D. M. Paul, and R. P. Singh, Unconventional superconductivity in La_7Ir_3 revealed by muon spin relaxation: Introducing a new family of noncentrosymmetric superconductor that breaks time-reversal symmetry, *Phys. Rev. Lett.* **115**, 267001 (2015).
- [27] T. Shang, S. K. Ghosh, J. Z. Zhao, L.-J. Chang, C. Baines, M. K. Lee, D. J. Gawryluk, M. Shi, M. Medarde, J. Quintanilla, and T. Shiroka, Time-reversal symmetry breaking in the noncentrosymmetric Zr_3Ir superconductor, *Phys. Rev. B* **102**, 020503(R) (2020).
- [28] R. P. Singh, A. D. Hillier, B. Mazidian, J. Quintanilla, J. F. Annett, D. M. Paul, G. Balakrishnan, and M. R. Lees, Detection of time-reversal symmetry breaking in the noncentrosymmetric superconductor Re_6Zr using muon-spin spectroscopy, *Phys. Rev. Lett.* **112**, 107002 (2014).
- [29] T. Shang, G. M. Pang, C. Baines, W. B. Jiang, W. Xie, A. Wang, M. Medarde, E. Pomjakushina, M. Shi, J. Mesot, H. Q. Yuan, and T. Shiroka, Nodeless superconductivity and time-reversal symmetry breaking in the noncentrosymmetric superconductor $\text{Re}_{24}\text{Ti}_5$, *Phys. Rev. B* **97**, 020502(R) (2018).
- [30] T. Shang, M. Smidman, S. K. Ghosh, C. Baines, L. J. Chang, D. J. Gawryluk, J. A. T. Barker, R. P. Singh, D. M. Paul, G. Balakrishnan, E. Pomjakushina, M. Shi, M. Medarde, A. D. Hillier, H. Q. Yuan, J. Quintanilla, J. Mesot, and T. Shiroka, Time-reversal symmetry breaking in Re-based superconductors, *Phys. Rev. Lett.* **121**, 257002 (2018).
- [31] W. Xie, P. R. Zhang, B. Shen, W. B. Jiang, G. M. Pang, T. Shang, C. Gao, M. Smidman, and H. Q. Yuan, CaPtAs : a new noncentrosymmetric superconductor, *Sci. China-Phys. Mech. Astron.* **63**, 237412 (2020).
- [32] T. Shang, C. Baines, L.-J. Chang, D. J. Gawryluk, E. Pomjakushina, M. Shi, M. Medarde, and T. Shiroka, $\text{Re}_{1-x}\text{Mo}_x$ as an ideal test case of time-reversal symmetry breaking in unconventional superconductors, *npj Quantum Mater.* **5**, 76 (2020).
- [33] T. Shang, W. Xie, J. Z. Zhao, Y. Chen, D. J. Gawryluk, M. Medarde, M. Shi, H. Q. Yuan, E. Pomjakushina, and T. Shiroka, Multigap superconductivity in centrosymmetric and noncentrosymmetric rhenium-boron superconductors, *Phys. Rev. B* **103**, 184517 (2021).
- [34] Y. P. Yarmolyuk and E. I. Gladishevskii, New ternary compounds of equiatomic composition in the systems of two transition metals and silicon or germanium, *Dopov. Akad. Nauk Ukr. RSR, Ser. B*, **11**, 1030 (1974).
- [35] G. V. S. Rao, K. Wagner, G. Balakrishnan, J. Janaki, W. Paulus, R. Schöllhorn, V. S. Subramanian, and U. Poppe, Structure and superconductivity studies on ternary equiatomic silicides, $\text{MM}'\text{Si}$, *Bull. Mater. Sci.* **7**, 215 (1985).
- [36] A. Suter and B. M. Wojek, Musrfit: A free platform-independent framework for μSR data analysis, *Phys. Procedia* **30**, 69 (2012).
- [37] W. Barford and J. M. F. Gunn, The theory of the measurement of the London penetration depth in uniaxial type-II superconductors by muon spin rotation, *Physica C* **156**, 515 (1988).
- [38] E. H. Brandt, Properties of the ideal Ginzburg-Landau vortex lattice, *Phys. Rev. B* **68**, 054506 (2003).
- [39] S. Serventi, G. Allodi, R. De Renzi, G. Guidi, L. Romanò, P. Manfrinetti, A. Palenzona, C. Niedermayer, A. Amato, and C. Baines, Effect of two gaps on the flux-lattice internal field distribution: Evidence of two length scales in $\text{Mg}_{1-x}\text{Al}_x\text{B}_2$ from μSR , *Phys. Rev. Lett.* **93**, 217003 (2004).
- [40] R. Khasanov, A. Amato, P. K. Biswas, H. Luetkens, N. D. Zhigadlo, and B. Batlogg, SrPt_3P : A two-band single-gap superconductor, *Phys. Rev. B* **90**, 140507(R) (2014).
- [41] M. Tinkham, *Introduction to Superconductivity*, 2nd ed. (Dover Publications, Mineola, NY, 1996).
- [42] A. Carrington and F. Manzano, Magnetic penetration depth of MgB_2 , *Physica C* **385**, 205 (2003).
- [43] R. Khasanov, R. Gupta, D. Das, A. Leithe-Jasper, and E. Svanidze, Single-gap versus two-gap scenario: Specific heat and thermodynamic critical field of the noncentrosymmetric superconductor BeAu , *Phys. Rev. B* **102**, 014514 (2020).
- [44] T. Shang, D. J. Gawryluk, J. A. T. Verezhak, E. Pomjakushina, M. Shi, M. Medarde, J. Mesot, and T. Shiroka, Structure and superconductivity in the binary $\text{Re}_{1-x}\text{Mo}_x$ alloys, *Phys. Rev. Mater.* **3**, 024801 (2019).
- [45] T. Shang and T. Shiroka, Time-reversal symmetry breaking in Re-based superconductors: recent developments, *Front. Phys.* **9**, 270 (2021), and references therein.
- [46] T. Shang, W. Xie, J. Z. Zhao, Y. Chen, D. J. Gawryluk, M. Medarde, M. Shi, H. Q. Yuan, E. Pomjakushina, and T. Shiroka, Multigap superconductivity in centrosymmetric and noncentrosymmetric rhenium-boron superconductors, *Phys. Rev. B* **103**, 184517 (2021).
- [47] R. Kubo and T. Toyabe, A stochastic model for low-field resonance and relaxation, in *Magnetic Resonance and Relaxation. Proceedings of the XIVth Colloque Ampère*, edited by R. Blinc (North-Holland, Amsterdam, 1967) pp. 810–823.
- [48] A. Yaouanc and P. D. de Réotier, *Muon Spin Rotation, Relaxation, and Resonance: Applications to Condensed Matter* (Oxford University Press, Oxford, 2011).
- [49] R. K. Harris, E. D. Becker, S. M. Cabral de Menezes, R. Goodfellow, and P. Granger, NMR nomenclature: Nuclear spin properties and conventions for chemical shifts, *Magn. Reson. Chem.* **40**, 489 (2002).
- [50] A. P. M. Kentgens, A practical guide to solid-state NMR of half-integer quadrupolar nuclei with some applications to disordered systems, *Geoderma* **80**, 271 (1997).

- [51] Nb has a 3g Wyckoff position, with an $m2m$ local symmetry, implying a single V_{zz} component. Nb is bonded in a 11-coordinate geometry to six Re and five Si atoms. There are two short- (2.87 Å) and four long (2.95 Å) Nb-Re bonds, as well as four short- (2.68 Å) and one long (2.78 Å) Nb-Si bonds. See: <https://materialsproject.org/materials/mp-1095061>.
- [52] J. Korringa, Nuclear magnetic relaxation and resonance line shift in metals, *Physica* **16**, 601 (1950).
- [53] E. Bauer, C. Sekine, U. Sai, P. Rogl, P. K. Biswas, and A. Amato, Absence of time-reversal symmetry breaking in the noncentrosymmetric superconductor $\text{Mo}_3\text{Al}_2\text{C}$, *Phys. Rev. B* **90**, 054522 (2014).
- [54] W. A. Hines and W. D. Knight, Spin-orbit coupling and nuclear magnetic resonance in superconducting metals, *Phys. Rev. B* **4**, 893 (1971).
- [55] D. Tay, T. Shang, Y. P. Qi, T. P. Ying, H. Hosono, H.-R. Ott, and T. Shiroka, s -wave superconductivity in the noncentrosymmetric $\text{W}_3\text{Al}_2\text{C}$ superconductor: An NMR study (2021), submitted to *J. Phys.: Condens. Matter*.
- [56] D. Hoult and R. Richards, The signal-to-noise ratio of the nuclear magnetic resonance experiment, *J. Magn. Reson.* **24**, 71 (1976).
- [57] A. M. Clogston, A. C. Gossard, V. Jaccarino, and Y. Yafet, Orbital paramagnetism and the Knight shift in transition metal superconductors, *Rev. Mod. Phys.* **36**, 170 (1964).
- [58] A. Pustogow, Y. Luo, A. Chronister, Y.-S. Su, D. A. Sokolov, F. Jerzembeck, A. P. Mackenzie, C. W. Hicks, N. Kikugawa, S. Raghu, E. D. Bauer, and S. E. Brown, Constraints on the superconducting order parameter in Sr_2RuO_4 from oxygen-17 nuclear magnetic resonance, *Nature* **574**, 72 (2019).
- [59] T. Shang, A. Amon, D. Kasinathan, W. Xie, M. Bobnar, Y. Chen, A. Wang, M. Shi, M. Medarde, H. Q. Yuan, and T. Shiroka, Enhanced T_c and multiband superconductivity in the fully-gapped ReBe_{22} superconductor, *New J. Phys.* **21**, 073034 (2019).
- [60] T. Shang, W. Xie, D. J. Gawryluk, R. Khasanov, J. Z. Zhao, M. Medarde, M. Shi, H. Q. Yuan, E. Pomjakushina, and T. Shiroka, Multigap superconductivity in the Mo_5PB_2 boron-phosphorus compound, *New J. Phys.* **22**, 093016 (2020).
- [61] A. Gurevich, Iron-based superconductors at high magnetic fields, *Rep. Prog. Phys.* **74**, 124501 (2011), and references therein.
- [62] N. R. Werthamer, E. Helfand, and P. C. Hohenberg, Temperature and purity dependence of the superconducting critical field, H_{c2} . III. Electron spin and spin-orbit effects, *Phys. Rev.* **147**, 295 (1966).
- [63] V. G. Kogan, C. Martin, and R. Prozorov, Superfluid density and specific heat within a self-consistent scheme for a two-band superconductor, *Phys. Rev. B* **80**, 014507 (2009).
- [64] N. Kimura, K. Ito, H. Aoki, S. Uji, and T. Terashima, Extremely high upper critical magnetic field of the noncentrosymmetric heavy fermion superconductor CeRhSi_3 , *Phys. Rev. Lett.* **98**, 197001 (2007).
- [65] I. Sugitani, Y. Okuda, H. Shishido, T. Yamada, A. Thamizhavel, E. Yamamoto, T. D. Matsuda, Y. Haga, T. Takeuchi, R. Settai, and Y. Onuki, Pressure-induced heavy-fermion superconductivity in antiferromagnet CeIrSi_3 without inversion symmetry, *J. Phys. Soc. Jpn.* **75**, 043703 (2006).
- [66] K. Okuda, M. Kitagawa, T. Sakakibara, and M. Date, Upper critical field measurements up to 600 kG in PbMo_6S_8 , *J. Phys. Soc. Jpn.* **48**, 2157 (1980).
- [67] F. F. Balakirev, T. Kong, M. Jaime, R. D. McDonald, C. H. Mielke, A. Gurevich, P. C. Canfield, and S. L. Bud'ko, Anisotropy reversal of the upper critical field at low temperatures and spin-locked superconductivity in $\text{K}_2\text{Cr}_3\text{As}_3$, *Phys. Rev. B* **91**, 220505(R) (2015).
- [68] J.-K. Bao, J.-Y. Liu, C.-W. Ma, Z.-H. Meng, Z.-T. Tang, Y.-L. Sun, H.-F. Zhai, H. Jiang, H. Bai, C.-M. Feng, Z.-A. Xu, and G.-H. Cao, Superconductivity in quasi-one-dimensional $\text{K}_2\text{Cr}_3\text{As}_3$ with significant electron correlations, *Phys. Rev. X* **5**, 011013 (2015).
- [69] H. Zuo, J.-K. Bao, Y. Liu, J. Wang, Z. Jin, Z. Xia, L. Li, Z. Xu, J. Kang, Z. Zhu, and G.-H. Cao, Temperature and angular dependence of the upper critical field in $\text{K}_2\text{Cr}_3\text{As}_3$, *Phys. Rev. B* **95**, 014502 (2017).
- [70] Z.-T. Tang, Y. Liu, J.-K. Bao, C.-Y. Xi, L. Pi, and G.-H. Cao, Anisotropic upper critical magnetic fields in $\text{Rb}_2\text{Cr}_3\text{As}_3$ superconductor, *J. Phys.: Condens. Matter* **29**, 424002 (2017).
- [71] Z.-T. Tang, J.-K. Bao, Z. Wang, H. Bai, H. Jiang, Y. Liu, H.-F. Zhai, C.-M. Feng, Z.-A. Xu, and G.-H. Cao, Superconductivity in quasi-one-dimensional $\text{Cs}_2\text{Cr}_3\text{As}_3$ with large interchain distance, *Sci. China Mater.* **58**, 16 (2015).
- [72] H. Z. Zhi, T. Imai, F. L. Ning, J.-K. Bao, and G.-H. Cao, NMR Investigation of the Quasi-One-Dimensional Superconductor $\text{K}_2\text{Cr}_3\text{As}_3$, *Phys. Rev. Lett.* **114**, 147004 (2015).
- [73] J. Luo, J. Yang, R. Zhou, Q. G. Mu, T. Liu, Z.-a. Ren, C. J. Yi, Y. G. Shi, and G.-q. Zheng, Tuning the Distance to a Possible Ferromagnetic Quantum Critical Point in $\text{A}_2\text{Cr}_3\text{As}_3$, *Phys. Rev. Lett.* **123**, 047001 (2019).
- [74] J. Yang, J. Luo, C. J. Yi, Y. G. Shi, Y. Zhou, and G.-q. Zheng, Spin-Triplet Superconductivity in $\text{K}_2\text{Cr}_3\text{As}_3$, *Sci. Adv.* **7**, eabl4432 (2021).
- [75] K. P. Sajilesh and R. P. Singh, Superconducting properties of the non-centrosymmetric superconductors TaXSi ($X = \text{Re}, \text{Ru}$), *Supercond. Sci. Technol.* **34**, 055003 (2021).
- [76] M. Angst, R. Puzniak, A. Wisniewski, J. Jun, S. M. Kazakov, J. Karpinski, J. Roos, and H. Keller, Temperature and field dependence of the anisotropy of MgB_2 , *Phys. Rev. Lett.* **88**, 167004 (2002).
- [77] A. Gurevich, S. Patnaik, V. Braccini, K. H. Kim, C. Mielke, X. Song, L. D. Cooley, S. D. Bu, D. M. Kim, J. H. Choi, L. J. Belenky, J. Giencke, M. K. Lee, W. Tian, X. Q. Pan, A. Siri, E. E. Hellstrom, C. B. Eom, and D. C. Larbalestier, Very high upper critical fields in MgB_2 produced by selective tuning of impurity scattering, *Supercond. Sci. Technol.* **17**, 278 (2004).